Propagation of Propeller Tone Noise Through a Fuselage Boundary Layer

D. B. Hanson* and B. Magliozzi†
Hamilton Standard, Windsor Locks, Connecticut

In earlier experimental and analytical studies, it was found that the boundary layer on an aircraft could provide significant shielding from propeller noise at typical transport airplane cruise Mach numbers. In this paper, a new three-dimensional theory is described that treats the combined effects of refraction and scattering by the fuselage and boundary layer. The complete wave field is solved by matching analytical expressions for the incident and scattered waves in the outer flow to a numerical solution in the boundary-layer flow. The model for the incident waves is a near-field frequency-domain propeller source theory developed previously for free-field studies. Calculations for an advanced turboprop (prop-fan) model flight test at a Mach number of 0.8 show a much smaller than expected pressure amplification at the noise directivity peak, strong boundary-layer shielding in the forward quadrant, and shadowing around the fuselage. Results are presented showing the difference between fuselage surface and free-space noise predictions as a function of frequency and Mach number. Comparison of calculated and measured effects obtained in a prop-fan model flight test shows good agreement, particularly near and aft of the plane of rotation at high cruise Mach number.

Nomenclature

B = number of blades
B_D = chord-to-diameter ratio
A_n, B_n = unknown coefficients for boundary-layer wave
C_n, B_n = unknown coefficients for scattered wave
c_0 = ambient speed of sound
E = Br_T^3/π
G_{mn}, Q_{mn} = source wave coefficients [see Eq. (17)]
$H_n^{(1)}$ = Hankel function
J_n = Bessel function of first kind
k = ω/c_0
k_r = radial wavenumber [Eq. (8)]
k_0 = chordwise source wavenumber [Eq. (12)]
k_x = axial wavenumber
m = harmonic of blade passing frequency
M = Mach number of boundary-layer flow
M_x = flight Mach number
M_r = section relative Mach number
n = Fourier index for ϕ variation
p = acoustic pressure
P = radial variation of pressure
P_n = unit solution of boundary-layer equation
$r, r_1, r_0, r_T, r_f, r_E$ = radii (see Fig. 4)
t = time
t_b = thickness-to-chord ratio
U = background velocity of boundary-layer flow
x = axial coordinate, fixed to aircraft, positive in direction of flow
Y_n = Bessel function of second kind
z = radial coordinate in boundary layer [see Eq. (20)]
z_0 = radius ratio on propeller
ϕ, ϕ_1 = angles (see Fig. 4)
ϕ_s = phase lag due to blade sweep
ρ_0 = ambient density
ω = radian frequency
Ω = angular speed of propeller
Ψ_v = Fourier transform of chordwise thickness distribution

Superscripts

$( )'$ = ∂/∂_r
$( )^*$ = complex conjugate

Presented as Paper 84-0248 at the AIAA 22nd Aerospace Sciences Meeting, Reno, Nev., Jan. 9-12, 1984; received March 15, 1984; revision received Aug. 16, 1984.

*Principal Research Engineer.
†Senior Analytical Engineer, Aircraft Systems Division. Member AIAA.

Introduction

THE advanced turboprop (prop-fan) has been in technology development since 1976 as a fuel-efficient propulsor for the 1990's. As part of the development program, a free-field noise theory[1] based on the acoustic analogy was developed and found to agree well with 1977 test results from an open-jet wind tunnel.[2] In 1981, a prop-fan model was installed on a business aircraft as shown in Fig. 1 for flight noise tests. Microphones were mounted flush with the fuselage surface in axial and circumferential arrays, as shown in Fig. 2. Because of the small wavelength of the sound and the large fuselage diameter, it was expected that the free-space sound levels directly beneath the propeller would be roughly doubled by reflection. However, it was found in early tests that free-space theory, with the 6 dB correction for pressure doubling, overpredicted measurements by 10 dB or more under some conditions.

After investigating several possible explanations for this overprediction, a simple analysis of the effect of the fuselage boundary layer on incoming acoustic waves[3] was developed that showed a powerful shielding effect at the high flight Mach number ($M_x = 0.8$) of the test. The early analysis was two-dimensional and treated plane waves impinging on a boundary layer over a rigid plane surface. Results for both step and linear boundary-layer profiles were given. McAninch,[4] whose analysis included the refinements of a near-field source and a curved boundary-layer profile, also concluded that significant shielding could occur.

This paper presents an extension of the original theory[3] to include effects of three-dimensionality; a near-field, distributed, rotating source; and an arbitrary boundary-layer profile using the geometry sketch in Fig. 3. The fuselage is

modeled as an infinitely long, rigid, circular cylinder with a boundary layer whose properties are constant along its length and circumference.

Theoretical Method

The problem described above will be solved by dividing the flowfield into a boundary-layer region and an outer region assumed to be free of shear. Waves in these two regions will be matched at the boundary-layer edge. Following methods given by Morse,[5] the outer wave field is constructed analytically from an incident wave appropriate to the source and a scattered wave in the standard Hankel function form. For the incident wave, a frequency-domain propeller radiation theory already exists[1] that is ideally suited to this analysis: its analytical form is in terms of the same Fourier components that occur naturally in the scattered wave and boundary-layer wave descriptions so that matching the fields is easily accomplished.

In the boundary-layer region, the wave equation must be solved by numerical methods because of the shear term. Over most of the axial wavenumber range, this is easily accomplished with standard numerical integration methods. However, for large positive wavenumbers, the wave equation acquires a singular point and special methods are required. Treatment of this singular point for the corresponding incompressible equation has received considerable attention in the past by Tollmien,[6] Lin,[7] and Wasow[8] in conjunction with boundary-layer instability theory. In more recent times, Tam and Morris[9] have addressed the full compressible equation in the analysis of radiation from shear-layer instability waves and pointed out that a Frobenius series can be used in the vicinity of the singular point. All of these investigators concluded that when the problem is imbedded in the complex plane, the singular point must be spanned by passing beneath it. Treatment of the singular point herein is in accord with the above references.

To establish the general form of waves in axisymmetric shear flow, consider the fuselage-centered coordinates in Fig. 4 with positive x measured downstream from the propeller plane of rotation. If the undisturbed velocity U is parallel to the x axis and is a function of r only, then the acoustic pressure outside the source region is given by Goldstein's[10] Eq. (1.2.2).

$$\frac{\mathrm{D}}{\mathrm{D}t}\left(\nabla^2 p-\frac{1}{c_0^2}\frac{\mathrm{D}^2}{\mathrm{D}t}p\right)-2U'\frac{\partial p'}{\partial x}=0 \tag{1}$$

where primes denote $\partial/\partial r$ and the convective derivative is

$$\frac{\mathrm{D}}{\mathrm{D}t}=\frac{\partial}{\partial t}+U\frac{\partial}{\partial x} \tag{2}$$

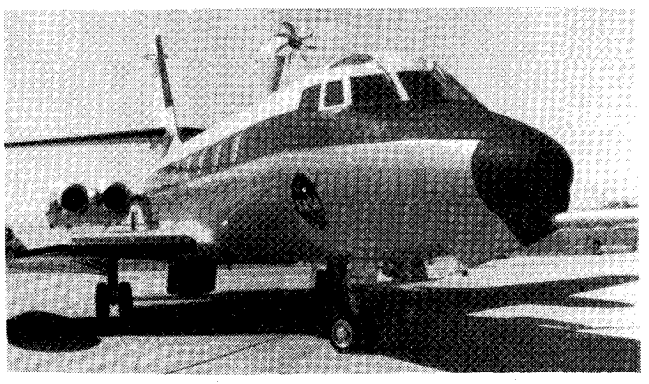

Fig. 1 Flying test bed for model prop-fans.

It is easily demonstrated that Eq. (1) admits elementary solutions in cylindrical coordinates of the form

$$P(r)e^{ik_x x}e^{in\phi}e^{-i\omega t} \tag{3}$$

Since we are considering sound from a propeller with B blades and angular speed Ω, the frequency of the mth harmonic is given by $\omega=mB\Omega$, and solutions at this frequency can be constructed from linear combinations of Eq. (3) in the following general form.

$$P=e^{-imB\Omega t}\sum_{n=-\infty}^{\infty}e^{in\phi}\int_{-\infty}^{\infty}F_n(k_x)P(r)e^{ik_x x}\mathrm{d}k_x \tag{4}$$

where the coefficients F_n are to be found. The equation for the radial part of the solution, $P(r)$, can be found by substituting Eq. (3) into Eq. (1) with the Laplacian

$$\nabla^2=\frac{1}{r}\frac{\partial}{\partial r}\left(r\frac{\partial}{\partial r}\right)+\frac{1}{r^2}\frac{\partial^2}{\partial\phi^2}+\frac{\partial^2}{\partial x^2} \tag{5}$$

The result, with $M=U/c_0$, is

$$(Mk_x-k)\left(P''+\frac{1}{r}P'\right)-2k_xM'P'+(Mk_x-k)\left[(Mk_x-k)^2-\left(k_x^2+\frac{n^2}{r^2}\right)\right]P=0 \tag{6}$$

where $k=\omega/c_0$. At this point we change notation and consider the pressure to be normalized by $\rho_0 c_0^2$. Also, wavenumbers k and k_x and distances are referred to the boundary-layer thickness δ.

Construction of the Wave Field Outside the Boundary Layer

In the outer region the Mach number M is constant at the flight speed value M_x so that $M'=0$ and Eq. (6) reduce to

$$P''+\frac{1}{r}P'+\left[(M_xk_x-k)^2-\left(k_x^2+\frac{n^2}{r^2}\right)\right]P=0 \tag{7}$$

This is Bessel's equation with solutions $J_n(k_r r)$ and $Y_n(k_r r)$ where the radial wavenumber is

$$k_r=\sqrt{(M_xk_x-k)^2-k_x^2} \tag{8}$$

The combination of J_n and Y_n corresponding to outgoing waves is the Hankel function

$$H_n^{(1)}=J_n+iY_n \tag{9}$$

Thus, the scattered wave is given by

$$p_s=e^{-imB\Omega t}\sum_{n=-\infty}^{\infty}e^{in\phi}\int_{-\infty}^{\infty}E[C_n(k_x)+iD_n(k_x)]\times H_n^{(1)}(k_r r)e^{ik_x x}\mathrm{d}k_x \tag{10}$$

where the coefficients C_n+iD_n will be determined when the wave fields inside and outside the boundary layer are matched. The constant $E=Br_T^3/\pi$ has been extracted for later convenience.

For the incident wave, a solution in the form of Eq. (4) is easily adapted from an earlier paper by Hanson.[1] In Ref. 1,

formulas were derived for near-field noise of propellers in forward flight. The theory which treats steady monopole, dipole, and quadrupole sources convected along helicoidal paths via the acoustic analogy has been used routinely at Hamilton Standard since 1977 for propeller and prop-fan noise predictions. For economy of space, only the formula for monopole (thickness) noise is given here. However, with the information given, the solution for the other sources could be written down immediately.

For an observer translating with the propeller at flight Mach number M_x the pressure in the mth harmonic of blade passing frequency is given by

$$p_i = -iEe^{imB(\phi_I - \Omega t)} \int_{\text{root}}^{\text{tip}} B_D^2 t_b \int_{-\infty}^{\infty} e^{i\phi_s} (M_x k_x - k^2) \Psi_v^*(k_0) \times J_{mB}(k_r r_T z_0) H_{mB}^{(I)}(k_r r_I) e^{ik_x x} dk_x dz_0 \quad (11)$$

where

$$k_0 = \frac{2B_D r_T}{M_r} (M_x k_x - k) \quad (12)$$

$$\phi_s = \frac{-2r_T}{M_r} (Mk_x - k) \frac{MCA}{D} \quad (13)$$

and, as in Ref. 1, B is the number of blades, B_D the chord-to-diameter ratio, t_b the thickness-to-chord ratio, and Ψ_v the chordwise spatial Fourier transform of the airfoil section thickness distribution. ϕ_s is the phase lag due to sweeping a blade section back along the advance helix by an amount MCA. To establish Eq. (11) from Ref. 1, a change in notation was made: the k of Ref. 1 was changed to $-(M_x k_x - k)/k$ in the present notation and k_x is now the wavenumber of the sound field in the flight direction. In Ref. 1, k_x was the chordwise source wavenumber, a role presently filled by k_0.

In Eq. (11), the coordinate system is centered in the propeller axis. The observer is located at r_I, ϕ_I, and x. However, since the matching process is to be applied at the edge of the fuselage boundary layer, the coordinate system for Eq. (11) must be shifted from the propeller axis to the fuselage axis as shown in Fig. 4. A Bessel function identity suited for this is given in Ref. 11:

$$e^{im\phi_I} H_{mB}^{(I)}(k_r r_I) = \sum_{n=-\infty}^{\infty} H_{mB+n}^{(I)}(k_r r_{CL}) J_n(k_r r) e^{in\phi} \quad (14)$$

When substituted into Eq. (11), this gives

$$p_i = e^{-imB\Omega t} \sum_{n=-\infty}^{\infty} e^{in\phi} \int_{-\infty}^{\infty} P_{i,n}(r) e^{ik_x x} dk_x \quad (15)$$

where the radial dependence is given by

$$P_{i,n}(r) = E(M_x k_x - k)^2 J_n(k_r r) [G_{mn}(k_x) + iQ_{mn}(k_x)] \quad (16)$$

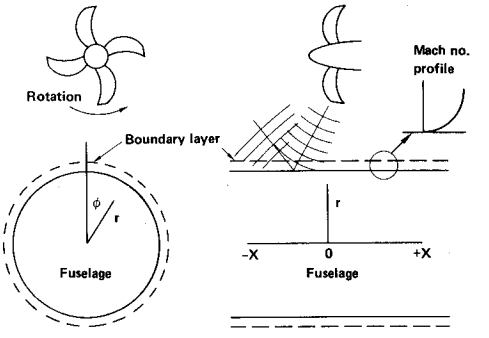

Fig. 3 Geometry treated in analysis.

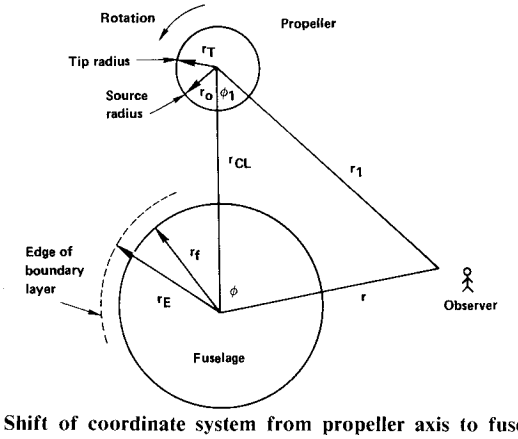

Fig. 4 Shift of coordinate system from propeller axis to fuselage axis.

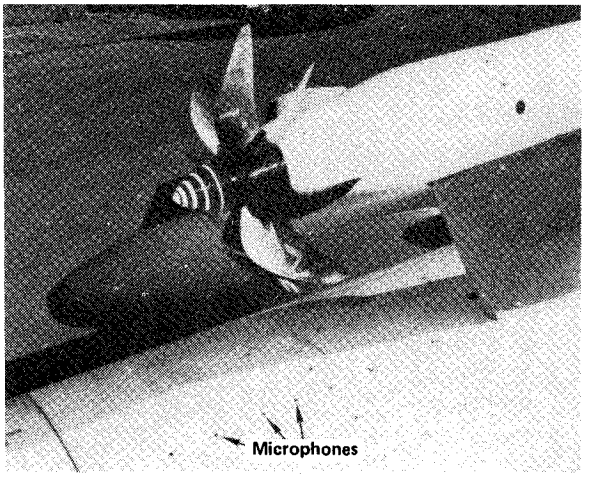

Fig. 2 Prop-fan model SR-3 mounted on Jetstar business aircraft showing microphone array.

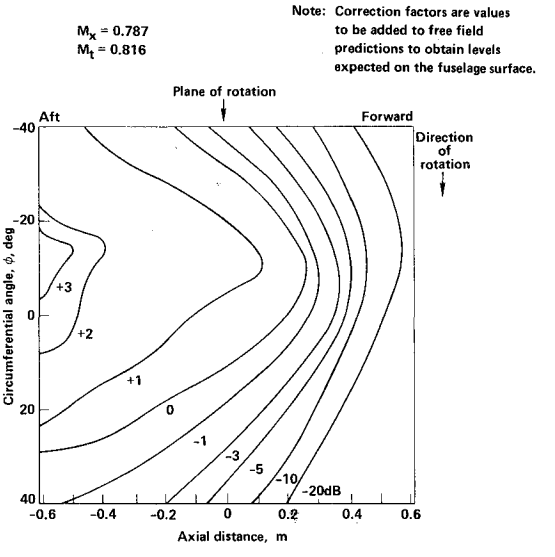

Fig. 5 Sample calculated correction factors for the Jetstar fuselage at blade passage frequency for an eight-blade prop-fan.

and

$$G_{mn}(k_x)+iQ_{mn}(k_x)=-iH^{(1)}_{mB+n}(k_r r_{CL})\times\int_0^l B_D^2 t_b e^{i\phi_s}\Psi_v^*(k_0)J_{mB}(k_r r_t z_0)\,dz_0 \quad (17)$$

Note that the integral in Eq. (17) contains all the source information.

In Eqs. (15-17), the incident pressure field has been decomposed into time, angle, and axial distance Fourier components. This has been done analytically by virtue of working in the frequency domain. In a time-domain source description, this threefold Fourier decomposition would have to be done numerically.

Computation of the Wave Field Inside the Boundary Layer

Pressure waves in the boundary layer are solutions to Eq. (6) subject to the appropriate boundary condition at the fuselage surface. Equation (6) is somewhat simplified here by dropping the P'/r term leaving

$$(Mk_x-k)P''-2k_xM'P'+(Mk_x-k)[(Mk_x-k)^2-(k_x^2+k_y^2)]P=0 \quad (18)$$

where, for n/r, we have written

$$k_y=n/\bar{r} \quad (19)$$

where $\bar{r}$ is the distance from the fuselage center to the middle of the boundary layer. This approximation is based on the fact that the fuselage radius is much larger than the boundary-layer thickness. Thus, the boundary-layer region will be solved on a plane in Cartesian coordinates and then "wrapped around" the fuselage. Periodicity in ϕ is guaranteed by requiring that n be an integer. This approximation could be eliminated easily, but it does not seem worthwhile at this point considering that the assumptions of a uniform boundary layer and a circular section fuselage are also approximate in most cases.

To solve Eq. (18), we shift the origin of the radial coordinate to the fuselage

$$r=r_f+z \quad (20)$$

so that the normal coordinate in the boundary layer is z, which runs from 0 at the fuselage to 1 at the boundary-layer edge. Over most of the range of interest in k_x, Eq. (18) is integrated by a standard Runge-Kutta method.

However, for $k_x>k/M_x$, the factor Mk_x-k goes to zero for some value of z between 0 and 1. This point, z_s, is a singular point of Eq. (18) and requires special treatment. The method used here is to apply the Runge-Kutta integration from $z=0$ to within a few mesh points of z_s where it is matched to a series solution about z_s. The series solution spans the singular point a few mesh points beyond z_s where the Runge-Kutta integration is continued to $z=1$.

For the series about z_s, we use the method of Frobenius[12] as suggested by Tam and Morris.[9] This is straightforward to apply and yields an indicial equation with roots equal to 0 and 3 so the two linearly independent series solutions are

$$P_A=(z-z_s)^3[1+a_1(z-z_s)+a_2(z-z_s)^2+\ldots] \quad (21)$$

$$P_B=1+b_1(z-z_s)+b_2(z-z_s)^2+\ldots+CP_A\ell n(z-z_s) \quad (22)$$

With two series, the numerical result can be matched for P and P'. The coefficients a_n, b_n, and C depend on the Mach number profile in the boundary layer and can be found by substitution into Eq. (18).

When the series in Eqs. (21) and (22) are matched to the numerical result on the fuselage side of the singular point ($z<z_s$), a decision must be made regarding branches of the log function. This issue has been discussed extensively in the literature in conjunction with studies of boundary-layer instability using the two-dimensional incompressible version of Eq. (18). The early works by Tollmien,[6] Lin,[7] and Wasow[8] are summarized by Schlichting,[13] where it is shown that the branch of the logarithm must be taken such that $\ell n(z-z_s)=\ell n|z-z_s|-i\pi$ for $z<z_s$. This was proved by examination of a more complete fourth-order differential equation for the flow that, because it includes viscosity, is not singular at z_s. Tam and Morris,[9] in their work on sound from compressible shear-layer instability waves, arrived at the same conclusion using different methods. They showed that the singular point may be spanned by embedding the problem in the complex plane and passing beneath z_s.

With respect to the form that waves may take in the vicinity of the critical layer ($z=z_s$), Tam and Morris'[9] analysis and the present analysis deal with different aspects of the same physical problem. Hence, we follow their precedent and use $\ell n(z-z_s)=\ell n|z-z_s|-i\pi$ for $z<z_s$.

For conditions with or without a singular point, unit solutions $\tilde{P}_n(k_x,z)$ to Eq. (18) for any k_x and n are obtained by integrating from $z=0$ to 1 starting with the following boundary conditions:

$$\tilde{P}_n(k_x,0)=1; \qquad \tilde{P}_n'(k_x,0)=0 \quad (23)$$

The general solution in the boundary-layer region is then

$$P_{BL}=e^{-imB\Omega t}\sum_{n=-\infty}^{\infty}e^{in\phi}\int_{-\infty}^{\infty}[A_n(k_x)+iB_n(k_x)]\times\tilde{P}_n(k_x,z)e^{ik_x x}\,dk_x \quad (24)$$

where $A_n(k_x)$ and $B_n(k_x)$ are to be found by matching to the outer field.

Matching of Equations at the Boundary-Layer Edge

We now have expressions for the wave field outside the boundary layer, P_s+P_i from Eqs. (10) and (15), and for the boundary-layer wave field P_{BL} from Eq. (24). These have to be matched at the boundary-layer edge $r=r_E$ for all x, ϕ, and t. Here the matching is achieved equivalently in the frequency/wavenumber domain for all k_x, n, and m. Thus, the matching equations for pressure and its derivative are

$$E[(M_xk_x-k)^2J_n(k_rr_E)(G_{mn}+iQ_{mn})+(C_n+iD_n)H_n^{(1)}(k_rr_E)]=(A_n+iB_n)\tilde{P}_n(k_x,1) \quad (25)$$

$$Ek_r[(M_xk_x-k)^2J_n'(k_rr_E)(G_{mn}+iQ_{mn})+(C_n+iD_n)H_n'^{(1)}(k_rr_E)]=(A_n+iB_n)\tilde{P}_n'(k_x,1) \quad (26)$$

The real and imaginary parts of these equations yield four equations that can be solved for A_n, B_n, C_n, and D_n, giving the entire wave field. In particular, Eq. (24) gives the pressure on the fuselage surface ($z=0$) with $\tilde{P}_n(k_x,0)=1$.

Amplification Plots

The theory derived above provides a means of predicting the absolute amplitude and phase of propeller noise on a

fuselage surface with a boundary layer. However, since the purposes of this study are to investigate the effects of the fuselage and boundary layer and to provide corrections to free-space levels, most results are presented as amplifications. Thus, 6 dB would represent the usual doubling effect of a hard wall; lower amplifications indicate boundary-layer shielding or fuselage shadowing.

Amplification is defined as the ratio (in decibels) between the acoustic pressure with fuselage and boundary layer, to the acoustic pressure at the same location in space but without the fuselage and boundary layer. Thus,

$$\text{Amplification} = 20 \log_{10} \left[\frac{(P_{BL})_{rms}}{(P_i)_{rms}} \right] \text{dB} \tag{27}$$

where both pressures are computed at $r = r_f$ and are functions of x and ϕ. In order to study fuselage effects without confusion due chordwise and spanwise interference within the propeller source, the blades were replaced by point sources at 80% of the blade radius. The chordwise thickness distribution is compressed to a point by using the chordwise transform for zero chord,

$$\Psi(k_0) = \Psi(0) \tag{28}$$

which is the ratio of the area of an airfoil section to the product of its chord and maximum thickness.

A plot of amplification as a function of x and ϕ for conditions typical of the JetStar/prop-fan model flight tests is shown in Fig. 5. Behind the plane of rotation, the combination of boundary-layer attenuation and finite fuselage diameter results in an amplification of about 4 dB (slightly less than the 6 dB expected for full pressure doubling). At forward locations, significant attenuation appears due to the boundary-layer refraction effects. Transverse to the airplane axis it can be seen that the peak amplification occurs at about -10 deg (see Fig. 5). This is a function of the direction of rotation of the prop-fan due to the source directivity. As would be expected, the amplification falls off on either side of the centerline because of grazing incidence.

Theory Verification

Although the amplification curves presented above exhibit the general behavior expected from previous experience with respect to shielding and shadowing effects, the theory was verified further in the numerical experiment described below.

First the scattering theory was checked by running some limiting cases with an infinitesimally thin boundary layer. The large wavelength behavior of the theory was verified by running at JetStar case with the fuselage diameter reduced to 0.0001 ft. The resulting amplification was less than 0.05 dB, indicating that a fuselage this small has negligible effect on the source field. In order to check the small wavelength of the theory, a fuselage diameter of 10 ft was used, producing an amplification of 6.0 dB. This is the same as the pressure doubling on an infinite plane, again verifying correct behavior. To check behavior at intermediate wavelength, comparisons were made with published curves for plane waves impinging on cylinders with no flow.[14] When plane waves were simulated by moving the source far from the fuselage, the predicted surface pressures matched those of Ref. 14.

Propagation within the boundary layer was checked by reproducing McAninch's two-dimensional amplitude results[4] for individual frequencies and wavenumbers. This was done by integrating Eq. (18) with $k_y = 0$.

Correlation with Model Prop-Fan Data in Flight

The available model data includes noise measurements made under actual high-speed, high-altitude flight conditions.

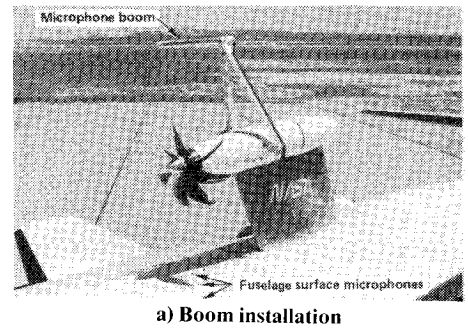

a) Boom installation

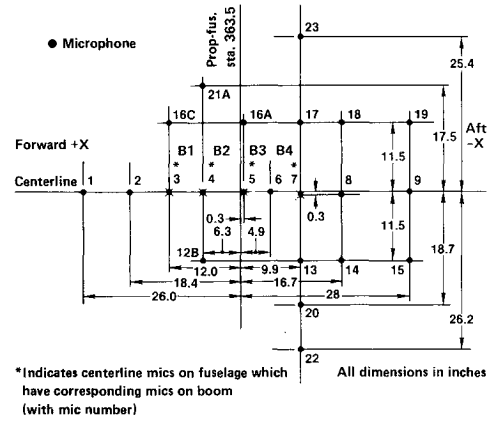

b) Microphone identification

Fig. 6 Jetstar microphone arrangement.

Model prop-fan noise was measured using microphones flush-mounted on the fuselage. Also, a limited number of test flights were made with a "free-field" microphone boom installed above the prop-fan. The microphone installations are shown in Fig. 6. Acoustic results from this series of tests were reported in Ref. 15.

The boom contained four microphones installed at axial locations and radial tip clearances corresponding to four microphone locations on the JetStar fuselage. Because of its thin boundary layer and small diameter (1.5 in.), it was expected that the boom noise levels would be representative of levels in free space and, therefore, would be useful for direct comparison with the fuselage levels. This turned out not to be the case, since the convection effect reduces the wavelength of noise at blade passing frequency to approximately 4 in., and significant scattering occurs at the boom. However, the present theory can be used to evaluate these effects by comparing the calculated noise at the boom and fuselage and then comparing that result with the corresponding measurements. This is readily seen from the relationship

$$\text{SPL}_B - \text{SPL}_{FS} = \Delta\text{SPL}_B \tag{29}$$

$$\text{SPL}_F - \text{SPL}_{FS} = \Delta\text{SPL}_F \tag{30}$$

where SPL_B is the sound pressure level at the boom microphone location, SPL_{FS} the free-space sound pressure level, and SPL_F is the sound pressure level at the fuselage microphone locations. Since the boom was located at the same distance from the prop-fan center as the fuselage, corresponding microphone locations have the same free-space sound pressure level. By equating SPL_{FS} in Eqs. (29) and (30), we obtain $\text{SPL}_B - \text{SPL}_F = \Delta\text{SPL}_B - \Delta\text{SPL}_F$. Thus, the measured SPL at the boom minus the measured SPL at the fuselage is equal to the difference between the boom effects and the fuselage effects. Since the latter is calculated by the

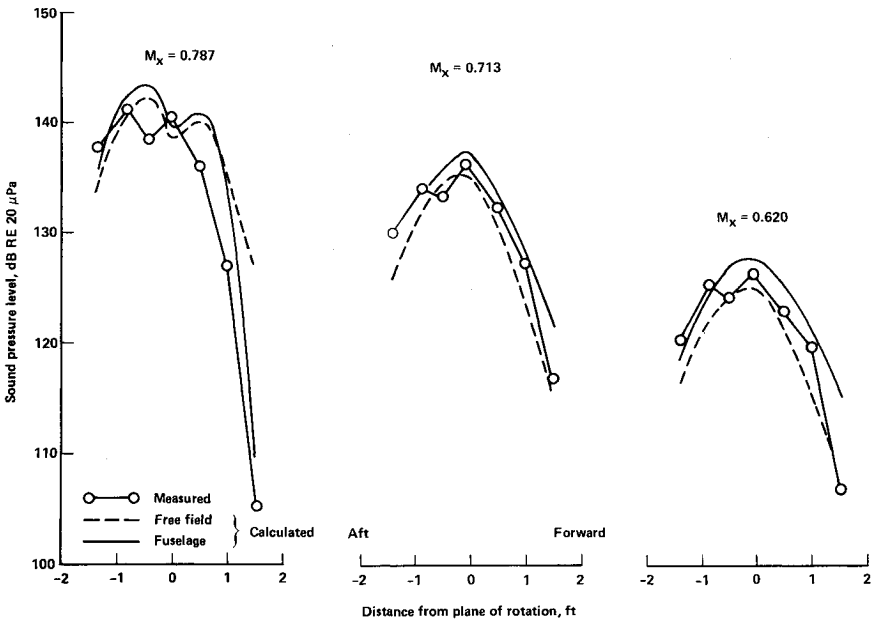

Fig. 7 Comparison of measured and calculated sound pressure levels at the Jetstar fuselage for SR-3.

Table 1 Comparisons of measured and calculated fuselage effects for the JetStar test airplane

Flight Mach No.	Harmonic	Microphone No. Boom/Fuselage	Measured SPL Boom	Measured SPL Fuselage	Calculated ΔSPL Boom	Calculated ΔSPL Fuselage	Measured Δ	Calculated Δ
0.787	1	1/3	133.1	127.0	2.3	−1.7	6.1	4.0
		2/4	—	136.0	2.8	0.5	—	2.3
		3/5	143.0	140.4	3.2	0.8	2.6	2.4
		4/7	146.1	141.3	3.2	1.3	4.8	1.9
	2	1/3	129.8	110.4	2.6	−14.9	19.4	17.5
		2/4	—	129.1	3.3	−2.4	—	5.7
		3/5	138.4	136.5	3.8	0.6	1.9	3.2
		4/7	137.9	136.3	4.2	0.5	1.6	3.7
	3	1/3	126.3	105.8	2.1	−21.9	20.5	23.0
		2/4	—	120.5	3.3	−5.2	—	8.5
		3/5	133.8	129.3	4.2	1.3	4.5	2.9
		4/7	135.8	118.6	4.6	0.3	17.2	4.3
0.710	1	1/3	139.0	137.8	1.6	4.6	1.2	−3.0
		2/4	145.6	142.0	2.1	3.0	3.6	−0.9
		3/5	145.0	142.5	2.3	1.9	2.5	0.4
		4/7	142.0	136.7	2.2	1.7	5.3	0.5
	2	1/3	131.6	128.9	3.8	7.4	2.7	−3.6
		2/4	137.6	135.0	4.0	4.3	2.6	−0.3
		3/5	138.8	139.6	4.1	1.8	−0.8	2.3
		4/7	141.1	125.8	4.5	1.1	15.3	3.4
	3	1/3	128.6	126.3	4.1	9.3	2.3	−5.2
		2/4	136.2	133.1	4.1	5.6	3.1	−1.5
		3/5	136.1	132.9	4.1	1.9	3.2	2.3
		4/7	130.9	121.4	4.2	0.2	9.5	4.0

present theory, a comparison can be made to evaluate the calculations. This approach has the advantage of not requiring that the prop-fan source characteristics be known. Table 1 shows comparisons for several representative conditions in the 0.6-0.8 flight Mach number range for the blade passing frequency hamonic of the SR-3 model.

As can be seen from comparison of the last two columns of Table 1, the agreement at $M_x = 0.787$ is generally good. The trend showing that the fuselage boundary-layer effects are stronger for the forward microphones is seen in both the measurements and calculations. At the lower flight speeds, the agreement is not as good. For the forward locations, the calculations show amplifications caused by boundary-layer refraction effects. The reason for these discrepancies which occur away from the peak directivity at the lower flight speed conditions will require further study.

Another way to evaluate the fuselage effects theory is to calculate free-space sound pressure levels, apply the fuselage correction, and then compare these with the measurements. Figure 7 shows comparisons between measured and calculated JetStar fuselage microphone data for the SR-3 model at BPF. The free-field source levels were calculated using Hanson's frequency domain method[1] and the fuselage corrections were calculated using the present analysis. As shown in Fig. 7, for a Mach number of 0.787, the boundary-layer propagation effects result in substantial attenuation at the forward microphone locations. At the more rearward microphones, the fuselage pressure amplification effects are about 1-2 dB. The strong attenuation is well borne out by the measurements. For the lower flight Mach number case, the method shows an increase over free-field levels for all measurement locations. In the aft locations, the increase is about 3-4 dB and is due to

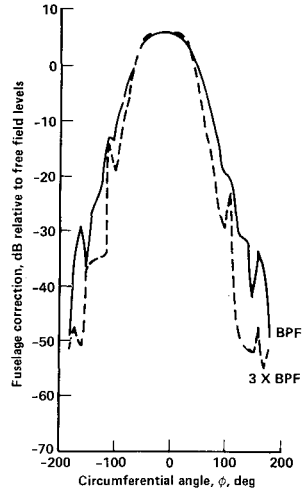

Fig. 8 Calculated fuselage scattering effects in plane of rotation at $M_x = 0.8$.

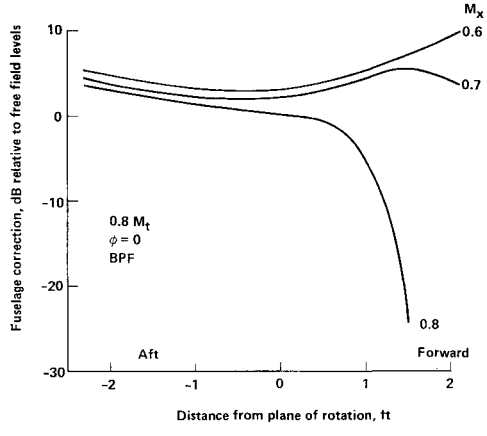

Fig. 9 Boundary-layer/fuselage effects vs flight Mach number at blade passing frequency.

pressure amplification caused by the fuselage. In the forward locations, the effect is about 5-7 dB. This appears to be a combination of fuselage reflection and a bending forward of the source directivity pattern by refraction in the boundary layer. This effect is somewhat overcalculated and it may be that the full source representation is needed rather than the rotating point sources used for generating correction curves. Generally, the agreement between measurements and calculations is improved by including the scattering and boundary-layer propagation effects.

Theoretical Trends

It is of interest to explore trends in fuselage effects with variations in operating parameters such as frequency and flight speed. Also, because the present theory includes fuselage scattering effects, it is possible to predict the variation of noise circumferentially around the fuselage.

Fuselage Scattering Effects

Figure 8 shows the calculated correction factor as a function of angle around a representative fuselage. This calculation was done assuming a negligible boundary layer for a flight Mach number of 0.8. Near 0 deg, the fuselage produces full pressure doubling. At positions around the fuselage, the pressure reinforcing effects decrease and beyond about 50 deg a shadow zone begins. On the opposite side of the fuselage, near 180 deg, a strong shadow zone may be seen. As expected, the shadow zone is stronger for 3XBPF than for BPF, because the wavelength is shorter for the higher frequency. Also, the 6 dB plateau is wider for the higher harmonic. Finally, it may be noted that the pattern is not

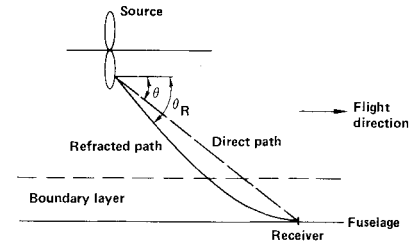

Fig. 10 Acoustic ray propagation through the boundary layer.

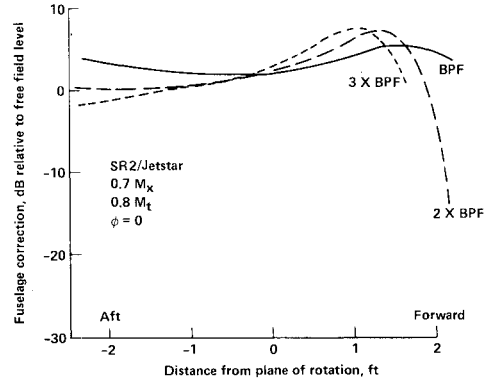

Fig. 11 Boundary-layer/fuselage effects vs frequency.

centered on 0 deg, but appears shifted by about 15 deg. This is a result of the prop-fan direction of rotation, as was also seen in Fig. 5.

Effect of Flight Speed

The boundary-layer refraction and fuselage scattering effects depend on flight Mach number as illustrated in Fig. 9. At a Mach number of 0.8, a modest pressure reinforcement appears aft of the plane of rotation. Forward of the plane of rotation, appreciable attenuation may be seen. The attenuation is caused by refraction effects in the boundary layer. At Mach numbers of 0.7 and 0.6, pressure reinforcement also appears aft of the plane of rotation. The effect initially decreases in the forward direction, but then appears to increase again. The 0.7 Mach number curve appears to peak at about 1.5 ft, then shows a decrease. The 0.6 Mach number curve is still rising beyond the range calculated. At 2 ft forward, the apparent fuselage effect is 9 dB. This is greater than would be expected from a pressure amplification effect. A possible explanation for this is that the propagation through the boundary-layer results in an apparent change in source directivity as illustrated in Fig. 10. In the absence of any boundary layer, the acoustic ray would travel to the receiver following the direct path. For the effective radius source represented, the directivity angle is indicated as θ. With the boundary layer present, the acoustic ray is refracted and follows the path labeled "refracted path." As shown, the refracted ray is at a directivity angle θ_R which is closer to the plane of rotation than angle θ. The source characteristics are such that the noise peaks near the visual plane of rotation, so that there is significantly more noise along θ_R than θ. The receiver then observes more noise due to the apparent directivity change caused by the refraction effects. At higher flight speeds, or at further forward positions, refraction is complete and the sound is greatly attenuated before reaching the receiver. Apparently, for the 0.7 Mach number curve in Fig. 9, the peak at 1.5 ft forward is due to the directivity change caused by the boundary-layer refraction effects. The correction then decreases again, as refraction becomes more complete.

Frequency Effects

The calculated fuselage boundary-layer effects are shown in Fig. 11 as a function of frequency. For this illustration, the effects were calculated for a flight Mach number of 0.7. The effects of frequency are seen in the three harmonics of blade passing frequency calculated. At low frequency, the behavior is as discussed previously. At 2XBPF, the peak has moved aft, consistent with a sharper source directivity. It can be seen that beyond 1.5 ft, the exponential decay effect has occurred, because full refraction through the boundary layer is occurring. At 3XBPF, the peak is still further aft.

Conclusions

A new theoretical method has been developed to correct free-field propeller noise measurements and predictions for the presence of a fuselage and its boundary layer. Incident waves are calculated from a verified near-field propeller source theory. Effects of scattering by the fuselage/boundary layer and refraction in the boundary layer are rigorously accounted for. In order to evaluate fuselage effects in general, without the complexity of chordwise and spanwise interference within the source, the propeller representation was reduced to a rotating point source for each blade. As expected from previous experience, the theory predicts strong attenuation forward of the propeller at cruise Mach numbers such as 0.8. Also, shadow regions are generated on the side of the fuselage away from the propeller. At a cruise Mach number of 0.8, the theory predicts only a 1 dB amplification of the noise directivity peak rather than the 6 dB that would be expected from simple pressure doubling.

Comparison of calculations with measurements obtained at a high cruise Mach number for a prop-fan model on a business jet aircraft show good agreement. At lower flight speeds, the theory shows amplification at forward angles that may be due to apparent source directivity changes caused by refraction in the boundary layer. This aspect of the predictions is not in good agreement with the data and it is possible that the more complete source description of the general theory should be used rather than the point source reresentation.

The calculated fuselage scattering/boundary-layer refraction effects show a strong dependence on frequency. In the region aft of the plane of rotation the pressure reinforcement effects approach 6 dB at higher frequencies. In the forward direction, the refraction effects result in substantial attenuation that becomes larger with increasing frequency.

Acknowledgments

The work described in this paper was supported by Contract NAS2-11325 from NASA Ames Research Center, Dryden Flight Research Facility. The authors wish to acknowledge the guidance of Dr. Harold D. Meyer of Hamilton Standard in developing the method for integrating the shear-flow wave equation as described in this paper.

References

[1] Hanson, D. B., "Near-Field Frequency-Domain Theory for Propeller Noise," AIAA Paper 83-0688 (to be published in *AIAA Journal*).

[2] Brooks, B. and Metzger, F. B., "Acoustic Test and Analysis of Three Advanced Turboprop Models," NASA CR-159667, Jan. 1980.

[3] Hanson, D. B., "Shielding of Prop-Fan Cabin Noise by the Fuselage Boundary Layer," Hamilton Standard, Windsor Locks, Conn., Engineering Rept. HSER 8165, Aug. 24, 1981; also, *Journal of Sound and Vibration*, Vol. 92, No. 4, Feb. 22, 1984, pp. 591-598.

[4] McAninch, G. L., "A Note on Propagation through a Realistic Shear Layer," Letter to the Editor, *Journal of Sound and Vibration* Vol. 88, No. 2, 1983, pp. 271-274.

[5] Morse, P. M., *Vibration and Sound*, McGraw-Hill Book Co., New York, 1948.

[6] Tollmien, W., "The Production of Turbulence," NACA TM 609, 1931.

[7] Lin, C. C., "On the Stability of Two-Dimensional Parallel Flows," *Quarterly of Applied Mathematics*, Vol. 3, 1945, pp. 117-142 (Pt. I) and pp. 218-234 (Pt. II).

[8] Wasow, W., "The Complex Assymptotic Theory of a Fourth Order Differential Equation of Hydromechanics," *Annals of Mathematics*, Vol. 49, No. 4, Oct. 1948, pp. 852-871.

[9] Tam, C. K. W. and Morris, P. J., "The Radiation of Sound by the Instability Waves of a Compressible Plane Turbulent Shear Layer," *Journal of Fluid Mechanics*, Vol. 98, 1980, Pt. 2, pp. 349-381.

[10] Goldstein, M. E., *Aeroacoustics*, McGraw-Hill Book Co., New York, 1976.

[11] Abramowitz, M. and Stegun, I. A., ed., *Handbook of Mathematical Functions*, National Bureau of Standards, Washington, D. C., 1964.

[12] Korn, G. A. and Korn, T. M., *Mathematical Handbook for Scientists and Engineers*, McGraw-Hill Book Co., New York, 1968, pp. 257-260.

[13] Schlichting, H., *Boundary Layer Theory*, 7th Ed., McGraw-Hill Book Co., New York, 1979, pp. 438-450.

[14] Wiener, F. M., "Sound Diffraction by Rigid Spheres and Circular Cylinders," *Journal of the Acoustical Society of America*, Vol. 19, No. 3, May 1947, pp. 444-451.

[15] Brooks, B. M., *Analysis of Jetstar Prop-Fan Acoustic Flight Test Data*. Hamilton Standard, Windsor Locks, Conn., Engineering Rept. HSER 8882, Nov. 1983.